MSc in Photonics

PHOTONICS**BCN**

Universitat Politècnica de Catalunya (UPC)
Universitat Autònoma de Barcelona (UAB)
Universitat de Barcelona (UB)
Institut de Ciències Fotòniques (ICFO)

http://www.photonicsbcn.eu

Master in Photonics

MASTER THESIS WORK

OPTOMECHANICS USING LOCALIZED EXCITONS IN SUSPENDED CARBON NANOTUBES

Nicolás Morell Bennasser

Supervised by Prof. Adrian Batchtold and Dr. Antoine Reserbat-Plantey (ICFO)

Presented on date 10th September 2014

Registered at

Escola Tècnica Superior d'Enginyeria de Telecomunicació de Barcelona

Optomechanics using localized excitons in suspended carbon nanotubes

Nicolás Morell Bennasser
Optomechanics Group, Institute of Photonic Sciences, Av. Carl Friedrich Gauss, 3 08860 Castelldefels (Barcelona), Spain

E-mail: nicolasmorellb@icfo.es

Abstract. Carbon nanotubes have generated a huge research interest in the last two decades. It can be seen as a wire with a diameter of about 1 nm. Because of this reduced dimensionality, nanotubes offer unique scientific and technological opportunities as nanomechanical resonators. Such resonators pave the way for new sensing applications with unprecedented sensitivities [1,2].
The linewidth of localized excitons in semiconducting carbon nanotubes was recently demonstrated to be very narrow (<10 GHz) [5,6]. Once localized by an external potential or a defect, excitonic states combine long coherent times (10 ns) and bright emission lines. It is likely that excitons and the local mechanical stress are strongly coupled in carbon nanotubes, so that localized excitons are promising to up convert the mechanical motion to optical fields [21]. Coupling the mechanical motion of a nanotube to excitons is appealing: it holds promise for the detection of ultra-small displacements. Interestingly, in this limit, the physics is governed by the laws of quantum mechanics.
We study photoluminescence of ultra-clean suspended carbon nanotubes at low temperature and we propose original scheme to measure the mechanical vibration via the exciton lineshift.

Keywords: Carbon nanotube, Optomechanics, Strain-mediated coupling, Exciton, Nanofabrication.

1. Introduction: general guidelines

The goal of this master project is to fabricate ultraclean suspended nanotube mechanical resonator showing narrow bandwidth photoluminescence. Such device would combine mechanical degree of freedom (nanoresonator) with two-level optical emitter (bright exciton). A perspective of this work is the observation of optomechanical coupling between the nanotube motion and the exciton energy. This would be a first step to further investigate manipulation and generation of non-classical state of motion [23].
Carbon nanotubes (CNTs) were discovered in 1991 [3]. They consist in a graphene honeycomb sheet rolled up into a tube. Their diameter d_{CNT} is on the order of 1 nm and their length can go from 1 to 100 μm. Such a length/diameter ratio makes them to be considered as one dimensional system showing special mechanical [1,2] and optical properties [3,5,6].
Carbon nanotubes are crystalline structures. Electronic and optical properties of a crystal are defined by its lattice vectors. It defines the energetic available states for the electrons (electronic bands) and the forbidden states (band gap) Fig. 1. By absorbing the energy of a photon an electron can be promoted to the higher energy *conduction band* from the lower energy *valence band* creating a positive charge (*hole).* In carbon nanotubes the vector defining the lattice is the chiral vector or chirality (n,m) and it depends on how the graphene honeycomb is rolled up. Electronic properties of graphene are described by the energy dispersion relation shown in Fig. 1a called *Dirac cone*. When the graphene is rolled, confinement of the electrons makes their energetic states to be quantized [4]. Electronic bands of nanotubes are formed by cutting the Dirac cone as shown in the Fig 1a. This gives a 1D density of electronic states Fig. 1b.

Depending on the chirality they are *metallic* or *semiconducting* nanaotubes. In this work we are interested in semiconducting type, capable of emitting photoluminescence (PL).

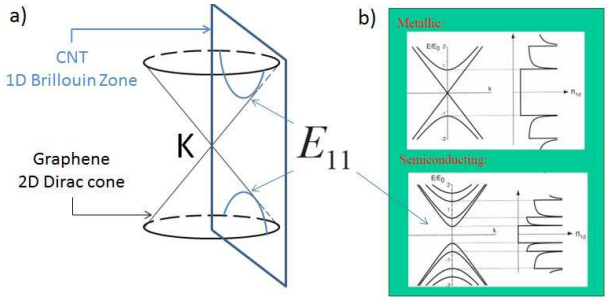

Figure. 1. a) Dirac cone in the central K point of the graphene reciprocal (momentum/Fourier) lattice. E_{11} is the lowest transition energy. b) Electronic bands and density of states for metallic (0 bandgap) and semiconducting nanotubes [3, 22].

Transitions between electronic bands are a first approach to describe optical transitions in carbon nanotubes. Nanotube electron-electron repulsion enlarges the bandgap and therefore blueshift the optical transitions. In addition, electron-hole coulomb attraction forms electron-hole pairs called *excitons* Fig. 2a. The difference in energy between the continuous conduction band and the exciton is the *exciton binding* energy. Binding energy and exciton energy increase inversely to d_{CNT} Fig. 2b. The large binding energy (up to eV for *subnanometric diameter* (<1 nm)) is the reason that excitonic and not band to band relaxations describe the optical emission of carbon nanotubes [3,13]. It has been shown that carbon nanotubes at cryogenic temperatures (4K) can act as a quantum light source (quatum dot-like) [5,6]. Their photoluminescence is well defined in energy/wavelength (μeV FWHM), long lifetimes (ns), long coherent times (ps), and show single photon emission (antibunching).

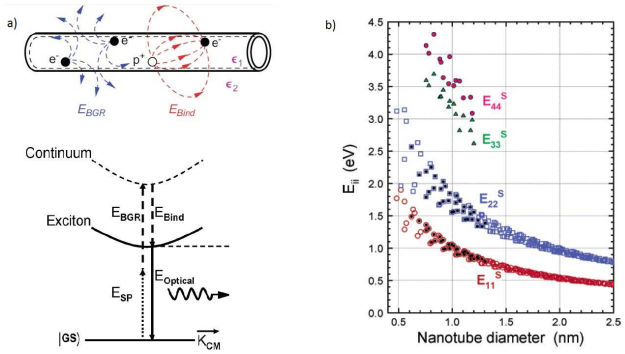

Figure 2. a) Coulomb interaction between confined particles induces bandgap renormalization and formation excitons (electron-hole pairs). b) *Katura Plot* shows the relation between the diameter and exciton energy (chirality) of a nanotube. (extracted from [3,13])

A way to obtain localized exciton emission is to isolate nanotubes from the environment [5,6]. This has been done by suspending them on trenches Fig. 4a. Even after massive development in carbon nanotube fabrication, it is still challenging to synthetize by chemical vapor deposition (CVD) nanotubes with fully precise control of the chirality/diameter and quality. CVD is a technique consisting on the catalytic decomposition of a carbon-based gas by metallic nanoparticles at high temperatures (500-1000ºC) [10,11]. In Fig. 3 commercial (CoMoCaT) a) and ultraclean CVD grown nanotube on SiO_2 substrate b) show ~15 meV and meV PL linewidth respectively in contrast with the μeV of CVD grown nanotube air suspended c). Suspended nanotube PL does not present variations in time (*spectral wandering*). Nanotube-nanotube interaction has also to be avoided as it quenches PL signal. The high tendency of nanotubes to form bundles Fig. 6 requires state of the art nano-fabrication techniques in order to get rid of them.

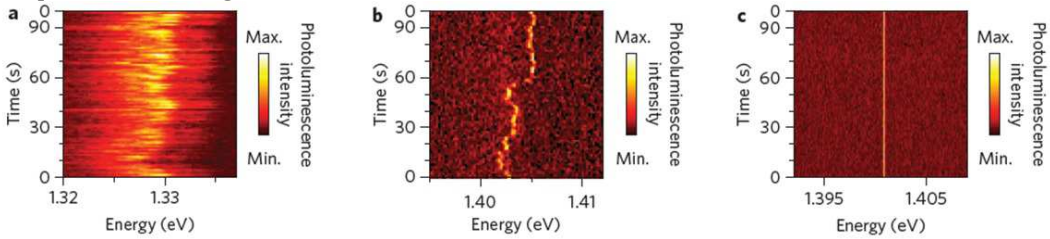

Figure 3: a), b) and c), show time trace of PL emission of: commercial (CoMoCaT, surrounded of surfactant molecules to avoid bundling), CVD grown ultraclean nanotube on silicon oxide substrate and CVD ultraclean suspended nanotube. Figure exracted from [5].

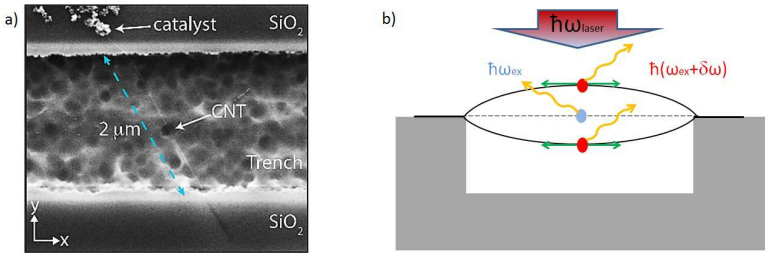

Figure 4. a) Electron micrograph of a sample with a carbon nanotube suspended over a SiO_2 trench. In b) motion elongates the nanotube lattice and modifies its PL emission.

Carbon nanotubes show mechanical resonant behaviour. This means that they vibrate with more amplitude at a certain frequency called resonant frequency ω_0. Carbon nanotube mechanical resonators are used for ultrasensitive measurements [1,2].
In Fig. 4a and Fig. 5a we see how the motion of a nanowire lead to a mechanical strain which locally modifies band structure and thus exciton energy [7,8]. This is the key element for strain mediated hybrid optomechanics It recently was shown Fig. 5 b how the mechanical motion at resonant frequency of a nanowire, changes the PL of a quantum dot embedded on it.

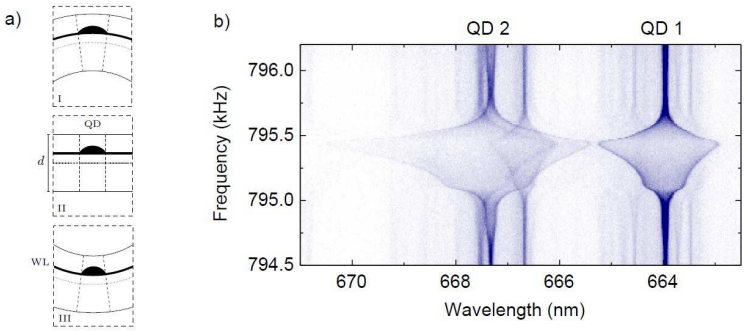

Figure 5. a) strain affects a material (quantum dot in a nanowire). b) Recent experimental result of strain-mediated modulation of PL of a quantum dot embedded in a nanowire, (figure extracted from [8,25]).

2. Ultraclean suspended carbon nanotubes: Materials and methods

Due to the exceptional mechanical [9], electrical [1,2,14], optical [5,6] and chemical [4,12] properties of CNTs strong research effort has been dedicated to its fabrication. CVD growth parameters such as catalyst particles diameter, composition, growth temperature or growth time can vary the diameter/chirality, density or quality of the nanotubes [5,6,10]. The large number of ill-defined parameters makes CVD nanotube growth difficult to control [10].
Brief description of the objectives and challenges (2.1), that such a complex sample raises, are firstly described. Then, I will introduce the state of the art techniques that have been used in all of the fabrication steps (2.2). And finally the characterization techniques used (2.3).

2.1. Fabrication challenges

Here is listed some of the main challenges in fabricating ultraclean suspended carbon nanotubes.

2.1.1 Ultraclean nanotubes

Defects like lattice dislocations, impurities or contamination affect both mechanical and optical properties of nanotubes [2, 5]. The term ultraclean in the carbon nanotube fabrication is used when the CVD growth happens at the last step of fabrication. Therefore, grown nanotube device is not exposed to any source of contamination (chemicals, metal evaporation, etc.). In

addition, to reduce to the limit the contamination chances, all processes are performed with extreme care and under *cleanroom conditions*.

2.1.2 Narrow diameter tubes

Because of the higher electron confinement their excitons present larger binding energy and larger excitonic energy Fig. 2b. We use a Si detector to record spectra and we are therefore limited to visible/ near IR emission, corresponding to subnanometer tubes.

2.1.3 Individual air suspended nanotubes

Nanotubes present a high tendency to form bundles Figure 6. Because of nanotube-nanotube non-radiative energy exchange, it can completely quench the PL emission. There are two strategies to avoid environment interaction: dispersing the carbon nanotubes in a surfactant solution or suspending/bridging them in air over trenches or pillars. Surfactant might alter optical and mechanical properties of nanotubes. Suspending SWNT in air is as far as known the best technique to isolate them. Nevertheless even if the substrate interaction is avoided, as shown in Figure 6, avoid the bundling tendency present a challenge. In order to get rid of bundling, control the density of suspended nanotubes by a deterministic placement of the catalyst particles is required.

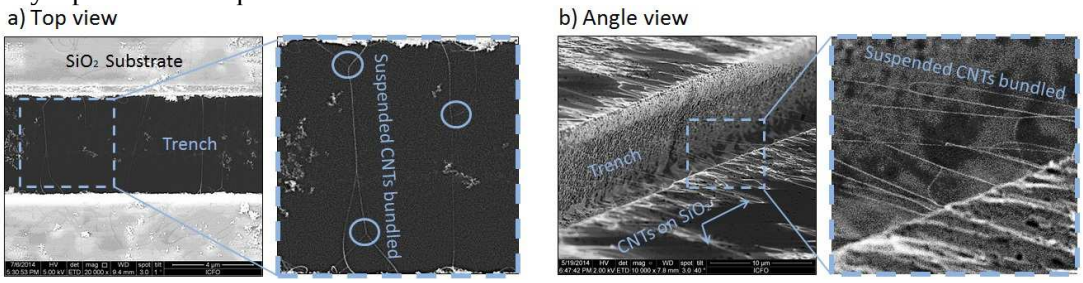

Figure 6. SEM picture of our samples sample, pictures are: taken from the top a), 45º angle b). CNTs suspended over 10 μm trenches and on t SiO_2 substrate. All nanotubes present bundling.

2.1.4 Long nanotubes

Long nanotubes (5-20 μm) have resonant frequencies of kHz- MHz and therefore can be excited with a commercial piezoelectric actuator. Another way to excite the mechanical motion of nanotubes is by electrical forces. Such way involves samples with electrodes and in addition high electric field can induce a doping effect in the tube, opening non radiative recombination channels.

2.2. Fabrication steps

The steps I have followed to develop the samples are explained below (see also Fig.7).

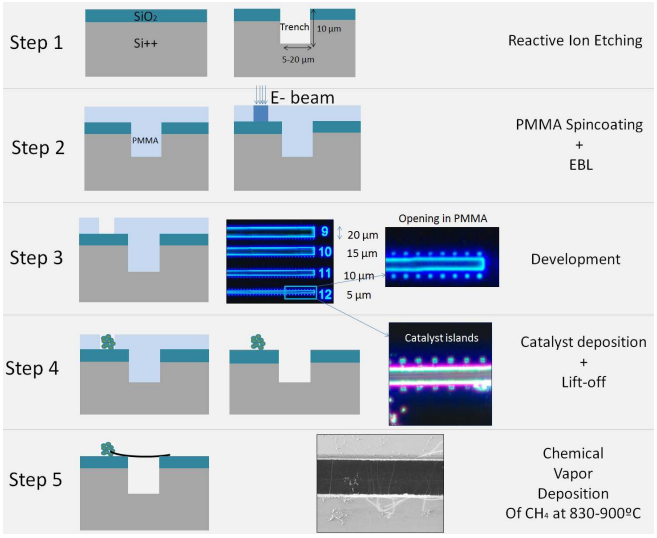

Figure 7. Step 1) RIE. Step 2) PMMA spin cast and EBL. Step 3) Development. Step 4) Catalyst deposition and Lift-off. Step 5) CVD. Pictures taken with dark field (DF).

Reactive ion etching. Fig. 7.1. It uses chemically reactive plasma (ion gas) to remove material deposited on wafers.

Deposition of the resist (preparation for electron beam lithography). This step consists in the deposition by spincast, of an electron sensitive resist Fig. 7.2. The resist used is polymethil methacrylate PMMA (950k-AR). The thickness of the resist layer (tens to hundreds of nm) can be tuned by changing the rotation speed and time. This process is non-trivial for rough structures like the one we studied (10 μm deep).

Electron beam lithography (EBL). Figure 7.2. In EBL, electrons are accelerated from a tungsten filament cathode by an electric potential and focused on the sample by magnetic lenses. This process allows exposing 10 nm resolution patterns. The dose of exposure (electron charge (μC)/area (cm^2)) and electron acceleration voltage has to be calibrated to not under or over-expose the resist. An accurate alignment of the e-beam write-field is needed in order to have a deterministic exposure.

Development. The electron beam change the solubility of PMMA and it can be easily removed with a specific solvent called developer. Fig. 7.3. The left PMMA forms a mask with 1μm^2 apertures.

Catalyst deposition. Just after the development, the catalyst solution is deposited on top of the sample. Catalyst particles precipitate on the surface and fill the holes created by EBL Fig. 7.4. This solution is composed by Fe as catalytic particles, Al_2O_3 support (where Fe sticks) and methanol as a solvent. A drop of solution is put on top of the sample; catalyst particles are deposited on the surface and fill the spots opened by previous steps. The methanol is removed by the capillarity of a piece of clean-room-paper and N_2 blow-drying. The sample is then baked at 150ºC between 5 and 15 min to completely remove the rests of methanol.

Lift-off. After the *catalyst deposition* the rest of the PMMA (with catalyst on top) mask is removed leaving catalyst particles only in the previously developed regions. This process called *lift-off* Fig. 7.4. Either 50ºC hot acetone or room temperature dichloreethane (DCE) can be used as solvent. This step has to be done with care to not remove the catalyst from the spots, increasing the probability of nanotube bundling.

Chemical vapour deposition (CVD). In this process, thermal decomposition of a CH_4 vapour is achieved in the presence of a metal catalyst. Nanotubes are supposed to grow in all directions from the catalyst islands created after lift-off and by chance some of them will be suspended over the trench Fig. 7.5. The temperature of growth (can vary from 800 to 1000ºC), time of growth (2-12 min) and gas flow are the parameters that can be changed to optimize the CVD growth.

2.3. Characterization

In this section, all techniques used to characterize fabrication of the final samples, are described.

2.3.1. Optical characterization: PL, Raman and PLE

Dark field microscopy (DF). DF consists on an optical microscope with high numerical aperture objective in which only rays arriving with a high incidence angle reach the samples surface and are scattered and collected. Even though it is limited by light diffraction and nanometric objects cannot be seen, it gives information of the surface roughness or position of catalyst islands.

Low temperature micro-photoluminescence (PL). PL spectra of carbon nanotubes are recorded using confocal (100×) setup. It allows observing individual nanotubes (diffraction limited spot of 500 nm diameter). Cryostat temperatures are as far as known the only conditions in which

nanotubes emit with narrow linewidth [5, 6]. With TiSa laser (750-950 nm) is possible to record the PL for different excitation wavelengths. This is called *excitation of the photoluminescence* and allows the reconstruction of the entire spectroscopy of the nanotube and therefore to fully determine its chirality. Despite its apparent qualities it presents some issues. It takes few seconds to record a conventional (non-micro) PL spectrum of an entire sample. In our case a 70 μm × 70 μm PL map takes about 10 hours.

Raman spectroscopy. Carbon nanotubes present characteristic phonon bands, each one corresponding to a different vibrational mode. They can be analysed by Raman spectroscopy [15,16]. This technique consists on optical excitation with a fixed wavelength, using a confocal microscope, and the detection of the energy shift of the sample emission with respect to this excitation. Is a non-linear scattering process in which phonon emitted (stokes) photons are detected and their energy is compared with the one of excitation. Every phonon band has a fixed Raman shift and gives information of a different property of the carbon nanotube. The main bands are the G-band, the radial breathing mode RBM-band and the D-band. The RBM is related to the radial vibration of the nanotubes and gives information of their diameter. The higher is the energy shift (Raman shift) the smaller the diameter, following the relation $\omega_{RBM}=C/d$ (cm^{-1}) where C=248 cm^{-1} nm is a constant for SWNT on a SiO_2 substrate [15]. The D-band is related to the defects in the nanotube, higher ratios D-band/G-band intensities come from nanotubes with high density of defects [17].
The main problem of this technique is that RBM are resonant Raman process, and full characterization of the sample requires sweeping laser wavelength.

Absorption spectroscopy. It consists on measuring the amount of light that a nanotube solution absorbs at each wavelength when is shined with white light Fig. 10b. To do such a measurement first nanotubes have to be put in solution with a surfactant molecule in order to separate bundles in *individual nanoubes*.

2.3.2. Other types of characterization: SEM and AFM

Scanning electron microscopy (SEM). The mechanism of SEM (2.2.3) is based on the scattering of electrons focused on the sample surface. It gives a standard resolution on the order of nm, not enough to determine d_{CNT} but enough to observe nanotubes and determine its density and degree of bundling Fig. 9a.

Atomic force microscopy AFM. This high-resolution ($\Delta z <$ nm) technique is based on a Si cantilever with a few nm size tip at its end. By probing the amplitude and/or frequency variations of the resonator, variations of the surface (like nanotubes) are detected. With AFM, characterization of the sample at all fabrication steps can be done, because it has enough resolution even to estimate the diameter of nanotubes Fig. 9b. Sample has to be scanned in maps of about 10 μm× 10 μm (1/6400 of the whole sample) that typically take few minutes. For subnanometer diameter the characterization of CVD grown nanotubes, is not precise enough to be concluding.

4. Results and discussion

In this section the main results of my thesis are presented and discussed.

4.1. Synthesis of ultraclean carbon nanotubes

In Fig. 9 I show the results referring to the quality of the nanotube samples. We characterize in first approach the level of surface contamination and the density of defects in the nanotubes by SEM micrographs. In Fig. 9a we see that SiO_2 is free of impurities that can be attached to the nanotubes during the CVD growth (dusts, solvent, grease or nanoparticles). To make a precise measurement of the surface roughness AFM measurements were performed.

Measured roughness of the surface Fig. 9b is below 200 pm (in the resolution limit of the AFM), 4 times lower than the nanotube diameter d_{CNT}. We can consider that this surface flatness has not been altered during the fabrication process as we reach the typical roughness of a base substrate.

Raman spectroscopy was used to determine the degree of purity of CVD grown nanotubes. We compared the G-band/D-band ratio between defected nanotube [17] and our CVD grown nanotubes presenting almost no defects Fig. 9c.

The time of growth was reduced from 10 min to 2 min producing the same density (1/µm) of suspended nanotubes. This way the probability to grow defects like amorphous carbon is reduced. For growths below 2 min no nanotubes were observed.

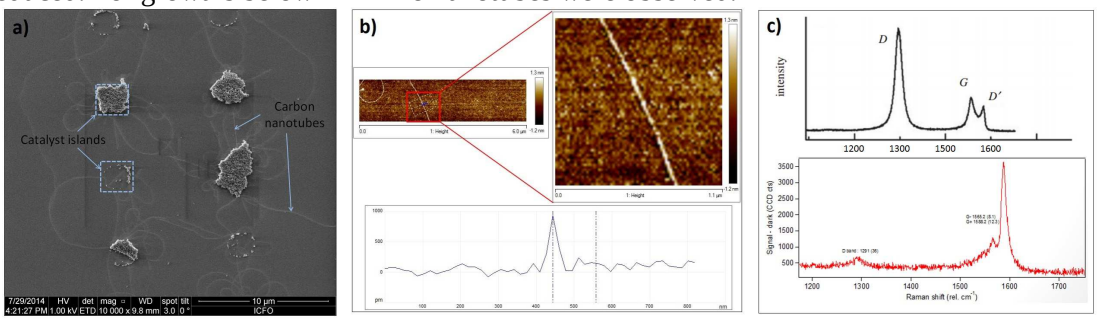

Figure 9. a) SEM micrograph of CVD grown nanotubes at 900ºC for 2 min in a flat substrate of SiO_2. 1µm ×1µm squares correspond to catalyst islands. b) AFM profile of an equivalent sample: nanotube (top) and its measured diameter d_{CNT}=0.8 nm with respect to the surface roughness 0.2 nm (bottom). c) Raman of defected (top, Extracted from [18]) and from our CVD nanotubes (bottom).

4.2. Production of high density of narrow diameter tubes

Diameter of nanotubes as a function of growth temperature was studied [10,11]. We characterized the d_{CNT} by Raman, AFM, absorption and low temperature PL. The last technique directly gives access to the chirality (and therefore to the diameter) (Section 2.3). Fig. 10a shows histograms of the tubes measured in micro-PL at low temperature. Values are compared with literature ones in order to address chirality and diameter. We do not observe a clear trend in the diameter distribution when growth temperature goes from 830 to 900ºC. Nevertheless, significant fraction of sub-nanometer nanotubes are observed ((6,4) and (6,2)).

We also attempted to characterize absorption spectra of nanotubes in solution with a surfactant. For *CoMoCaT* nanotubes Fig. 10b (red curve), shows 4 absorption peaks corresponding to nanotube chiralitys (5,3), (8,4), (8,3) and (11,0). But in CVD grown nanotubes (blue curve), only the base-line of the surfactant solution is observed. The reason is that it requires advanced techniques (ultracentrifugation and precise control of the solution molarity) to efficiently individualize nanotube from bundles and catalyst.

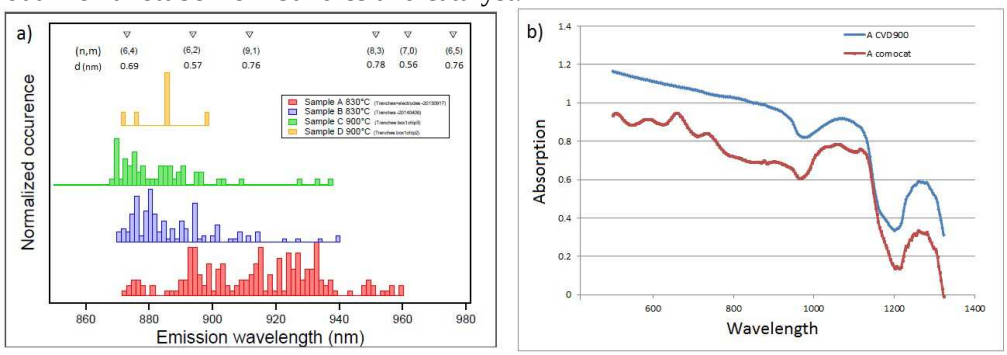

Figure 10. a) PL vs emission wavelength (corresponding to a diameter/chirality) histogram for different samples grown at (yellow and green) 900ºC and (red and blue) at 830ºC. b) Absorption spectra of nanotubes in surfactant solution, CVD (blue) and comocat (red).

After the study of different CVD temperatures, even though no concluding results on the nanotube diameter was found, we kept the 900ºC growth because it shows a higher density of nanotubes for the same amount of catalyst deposited Fig. 11.

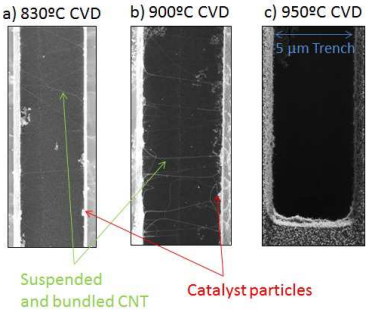

Figure 11. CNT samples with different growth temperatures showing different densities of suspended nanotubes are shown: (1) at 830, (2) at 900 and (3) at 950ºC. Higher density (over 1/ µm) of suspended nanotubes is observed for 900ºC growth and at 950ºC almost no nanotubes were found (below 1/100 µm)

4.3. Deterministic catalyst deposition to avoid bundling.

To produce individual nanotubes a deterministic deposition of the catalyst is needed. This requires: i) to cover the entire sample with a homogeneous layer of PMMA, ii) to expose with the right dose of electrons in the EBL and iii) optimizing the lift-off procedure. The two first objectives were attacked by testing different PMMA recipes (changing the resist, adding layers and changing the rotation speed of the spincast) and doing e-beam dose tests. In figure Fig. 13a a sample with the standard lift-off of 30 min in 50ºC hot acetone is shown. We can see that catalyst particles spread and some chunks of tens of microns, when is supposed to form 1µm× 1µm islands. To solve this problem, in flat SiO_2 samples we tested the effect on the lift-off (2.2) of putting the sample for few seconds in an ultrasonic bath after the 30 min in hot acetone. Results presented in Fig. 13 show an improvement of the lift-off as we increase the time of sonication. In Fig. 13a catalyst is spread almost forming a homogeneous layer, a sign that the lift-off didn't work. In Fig. 13b with 5 s of sonication, we can already see defined catalyst spots and some regions were the catalyst didn't lift. Lift-off with 7 s of sonication Fig. 13c present defined regions surrounded by perfectly clean substrate.

For most of the regions in Fig. 13c the lift-off worked but we see that the arrays of islands are not homogeneous. This means that during the catalyst deposition some of the EBL openings were not filled by catalyst particles. To improve catalyst deposition, we increased the time we let the catalyst particles in the solution fall to the sample surface homogeneously filling the openings (see catalyst deposition Section 2.2). Keeping the 7 s ultrasound bath lift-off, we increased from 1min (in the previous samples of Fig. 13) to 2 Fig. 13d and 3 min Fig. 13e. After the lift-off, catalyst remains in deterministic patterns keeping substrate clean Fig. 13f.

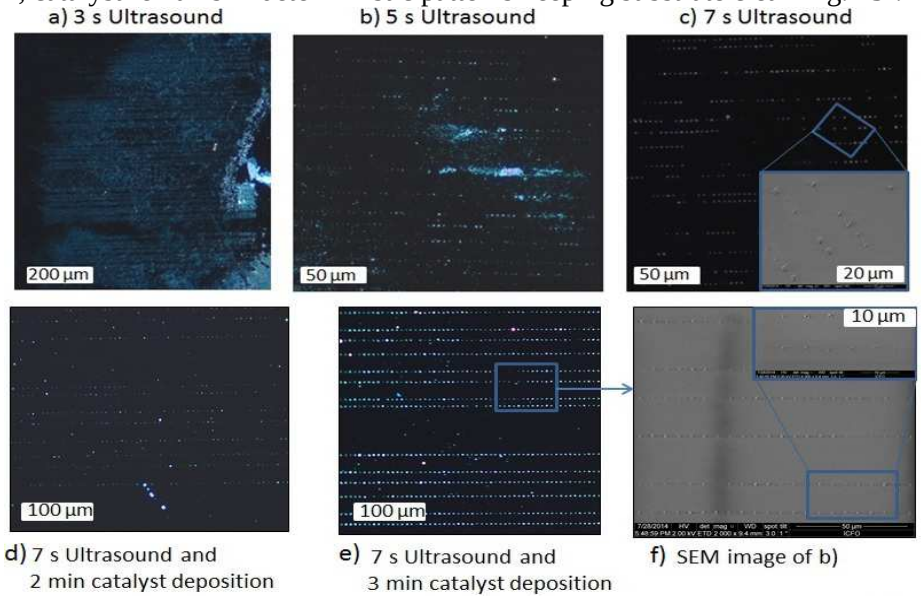

Figure 13. Dark field images of flat samples after lift-off using: a) 3 s of ultrasonic bath, b) 5 s of ultrasonic bath and c) 7 s of ultrasonic bath. Keeping 7 s ultrasound in a) sample catalyst drops rested for 2 min before the solvent was removed (2.2) and for 3 min for b). An SEM micrograph of b) is presented in c).

The next step was to try this method for samples with trenches. Results are shown in Fig. 14, where a sample with (**b)** and one without (**a)** the improvements in catalyst deposition and lift-off are compared.

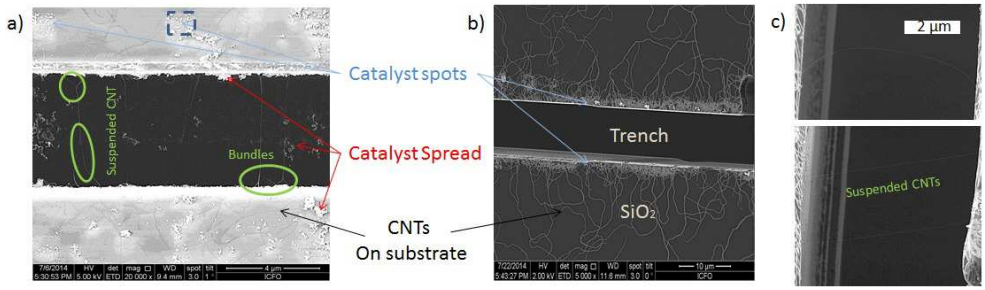

Figure 14. SEM pictures after CVD growth. In a) a sample with 1 min catalyst deposition and lift-off of 30s in 50ºC acetone is shown. In sample b) 3 min catalyst deposition and sonication after the 30s in 50ºC acetone. c) unbundled suspended nanotubes in sample b).

Previous method (a) produce samples with non-controlled catalyst positioning with high density of suspended nanotubes, but all of them bundled. With the 7 s ultrasound bath and 3 min catalyst deposition (b), also for the samples with trenches, catalyst islands are perfectly defined and rest of the substrate is clean. We observe a decrease in the density of suspended tubes b) with respect to a), present no bundling Fig. 14c.

4.4. Long nanotube synthesis

For samples with high catalyst surface density like the one on Fig. 14a suspended nanotubes with lengths up to 15 and 20 µm were observed. For samples Fig. 14b the density of suspended tubes nanotubes is lower (~1/20 µm) and the chance to find long nanotubes decrease. Longest nanotubes observed in these samples were 5-10 µm long and most of the tubes are 1-5 µm long.

4.5 Low temperature photoluminescence

Fig. 15 shows a PL spectrum of a suspended nanotube in a sample fabricated with the method described in this thesis.

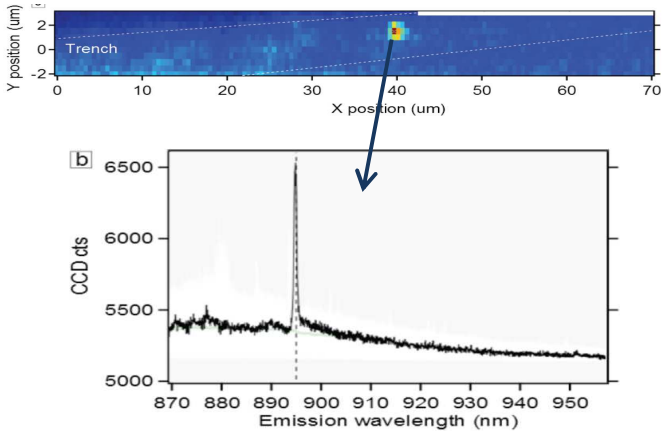

Figure 15. PL spectra showing meV bandwidth (botom) coming from the spot in the trench region of the PL map (top) taken in one of our samples.

5. Conclusions

In my thesis, I have shown fabrication procedure to synthetize suspended ultraclean nanotubes of narrow diameter has been presented. By AFM measurements and PL histograms we have shown that this process produces nanotubes with few defects and narrow diameter. I have presented an improvement of the catalyst deposition and lift-off procedures by increasing the deposition time of the catalyst and introducing the sample in an ultrasound bath respectively. This result have reduced the amount bundling and therefore increased the chance to observe suspended single wall nanotube PL. The reduction on the density of tubes might also reduce the amount of suspended nanotubes per sample but this can be solved by using smaller (1-4 μm) trenches. This work is part of a project aiming to observe optomechanical coupling between nanotube exciton and nanoresonator mechanical motion.

6. Perspectives

Alternative ways separate bundles and increase exciton localization might be studied: i) different catalyst solutions and densities [12] ii) creation of controlled defects to Engineer excitonic traps [24] iii) externally create potentials by applying an electric field,
Measure exciton energy while sweeping the mechanical drivingof the resonator would enable to probe and quantify the strain mediated coupling. This would constitute a milestone for further experiments: i) investigate effects of exciton population in the mechanical resonance and the other way around ii) optically manipulate the mechanical motion with real time readout iii) active sideband cooling of the resonator up to non-classical states of motion with the possibility of optical non-demolition measurements [19,20,23].

There's also he possibility to fabricate samples with electrically contacted nanotubes in order to electrostatically drive their motion and investigate the role of nanotube doping into the optomechanical coupling mechanism .

7. References.

[1] Moser *et al*. Nature Nano. 8, 493, (2013).
[2] J. Chaste *et al*. Nature Nano. 10.1038 (2012)
[3] Galland PhD Thesis, Swiss federal institute of technology, Zurich. arXiv (2011).
[4] Dresselhaus Physical properties of carbon nanotubes, Imperial College (1998)
[5] Hofmann *et al*. Nature Nano. 8, 502 (2013).
[6] Sarpkaya *et al*. Nature Comm 2152 (2013).
[7] Yeo *et al*. Nature Nano. 10, 1038 (2014).
[8] Montinaro *et al*. arXiv (2014).
[9] Poot *et al*. Physics Reports (2012)
[10] Kumar and Ando *et al*. Journal of Nanoscience and Nanotechnology 10, 3739–3758 (2010)
[11]Zoican Loebick *et al*. Journal American Chemical Society 132, 11125-11131 (2010)
[12] Ago *et al*. J. Phys. Chem. 109, 10035-10041 (2005)
[13] Weisman Nano Letters. 3, 9 (2003)
[14] Ando *et al*. Journal of the Physical Society of Japan 74, 3 (2005)
[15] Dresselhaus *et al*. Physics Reports 409 (2005)
[16] Htoon *et al*. PRL 94, 127403 (2005)
[17] Raman Graphite
[18] Dresselhauss *et al*. Phil. Trans. R. Soc. A 368 (2010))
[19] Aspelmeyer *et al*. Physics Today 65, 29 (2012)
[20] Schwab and Roukes *et al*. Physics Today (2005)
[21] Wilson-Rae *et al*. New Journal of Physics 14, 115003 (2012)
[22] F. Heinz, Recent Advances in the Optical Spectroscopy of CNT, (Columbia University, New York)
[23] Galland *et al*. PRL 112(14):143602. (2014)
[24] Gosh *et al*. Science 330, 1656 (2010)
[25] Wilson-Rae *et al*. PRL 92, 7 (2004)